Journal of Photochemistry and Photobiology A: Chemistry 337 (2017) 71–81

Contents lists available at ScienceDirect

Journal of Photochemistry and Photobiology A: Chemistry

journal homepage: www.elsevier.com/locate/jphotochem

Invited feature article

Synthesis of 13-substituted derivatives of berberine: Aggregation-induced emission enhancement and pH sensitive property

Xuemei Tang[a], Jianhui Zhang[b], Liyan Liu[a], Depo Yang[a], Huaqiao Wang[c,*], Feng He[a,*]

[a] School of Pharmaceutical Science, Sun Yat-sen University, Guangzhou 510006, China
[b] School of Chemistry, Sun Yat-Sen University, Guangzhou 510275, China
[c] Department of Anatomy and Neurobiology, Zhongshan School of Medicine, Sun Yat-Sen University, Guangzhou, Guangdong 510080, China

ARTICLE INFO

Article history:
Received 1 November 2016
Received in revised form 11 January 2017
Accepted 13 January 2017
Available online 19 January 2017

Keywords:
Berberine derivatives
Aggregation-induced emission enhancement
Crystal structure
Cell viability
pH sensitivity

ABSTRACT

Five kinds of berberine derivatives with hydroxy, methyl, ethyl, benzyl and (4-methyl)benzyl group at 13-position have been synthesized and characterized. 13-hydroxyberberine chloride exhibits aggregation-induced emission enhancement (AIEE) property because of hydroxy group, which is beneficial to increase the rigidity of molecule by enlarging conjugated system. Optical properties in pure solution, CH_3OH/H_2O mixed solution, amorphous and crystalline state were comparatively investigated. Polymeric morphology and particle size of 13-hydroxyberberine chloride with different water fractions (0–90 vol%) were obtained by scanning electron microscope (SEM) and dynamic light scattering (DLS) method respectively, which provided reasonable explanation that the formation of small globular nanoparticles in mixed solution is conducive to the fluorescence emission. The single crystal structure of 13-hydroxyberberine chloride was determined by single-crystal X-ray diffraction. Crystallographic data indicated that the main mechanism of the AIEE phenomenon is the existences of J-aggregation (head to tail dipole stacking) combined with molecular planarization. The calculation done by DFT showed that the HOMO–LUMO bandgap is in accordance with experimental data. To further explore the biomedical application of 13-hydroxyberberine, its cell viability and cell imaging performance were examined, which demonstrate that 13-hydroxyberberine shows definite fluorescent intensity. In all, 13-hydroxyberberine should be a promising candidate for different biomedical application such as pH fluorescence probe because of its response to the stimuli of pH value.

1. Introduction

As we all know, an increasing number of scientists pay more attention to the development of nano- and microsized fluorescent materials [1]. Fluorescent materials possess highly fluorescence efficiency in the state of nanoaggregation, solid and crystalline, namely aggregation-induced emission enhancement (AIEE) property, which is opposite to the "aggregation-caused quenching" (ACQ). Nevertheless, a majority of fluorescent materials are subjected to aggregation-caused quenching (ACQ) effect because of intensive π-π stacking and dipole–dipole interactions, which bring about low fluorescence emission, limiting the application of fluorescent materials. As a kind of AIE(E) fluorescent material, small organic molecules attract tremendous attention due to their strong emission in the poor solvents [2–4]. For example, siloles compound is considered as the most representative of an aggregation-induced emission (AIE) compound in earlier study of Tang's group [5]. Following closely behind are tetraphenylethylene (TPE) compound [6], intramolecular charge transfer (ICT) compound [7], and hydrogen bonding compound [8], which are also exploited as the new AIE molecules. Tang's group has also reported the luminescence mechanisms of AIE(E) which involve inter- and intramolecular phenomena, such as molecular conformation distortion, J-aggregation, C—H···π interaction and so forth [9–12].

Recently, this kind of organic molecule is considered to have great potential application in the field of photocatalysts [13], organic light-emitting diodes (OLEDs) [14,15] and optical devices [16], especially as chemical or biological probe [17]. Many important physiological processes of the body are related to pH

* Corresponding authors.
E-mail addresses: wanghq@mail.sysu.edu.cn (H. Wang), hefeng@mail.sysu.edu.cn (F. He).

http://dx.doi.org/10.1016/j.jphotochem.2017.01.017
1010-6030/

value, and the fluorescence property of some compounds can indicate the change of acid-base property of medium. Therefore, the study of fabricating novel chemical or biological fluorescence probe with AIE(E) molecules is valuable. In comparison to traditional pH fluorescence probe with the problem of aggregation-caused quenching (ACQ), new pH fluorescence probe has higher sensitivity and faster response speed [18,19].

Based on our previous researches [20–22], our group synthesized a series of 13-substituted derivatives of berberine (Scheme 1) and their spectroscopic properties in solution, nanosuspensions, amorphous and crystalline were investigated [23,24]. With further exploration of 13-hydroxyberberine chloride assembly feature, we researched its polymeric morphology and particle size by scanning electron microscope (SEM) and dynamic light scattering (DLS) method respectively. Crystal structure elucidates the mechanism of enhanced emission in the aggregation state. The geometrical and electronic structures were obtained to evidence the AIEE study of compound **1**. Moreover, the relationships between photoluminescence (PL) intensity and pH values were explored [25]. To further examine the biological potential of compound **1** as pH fluorescence probe, the cell uptake behavior as well as cell viability of it was further evaluated.

2. Experimental

2.1. Materials and instruments

All the reagents were obtained commercially, analytical grade and used without further purification. Berberine chloride, Sodium borohydride ($NaBH_4$), formaldehyde solution, benzyl bromide and acetaldehyde solution were obtained from Sigma-Aldrich, and 4-Methylbenzyl bromide was got from Macklin. NMR spectra were record on a Bruker Avance III 400 MHz spectrometer in DMSO-*d*6 as the internal standard. Mass spectra were measured on Shimazu LCMS-IT-TOF mass spectrometers. Ultraviolet (UV) absorption was recorded on a Shimadzu UV-2600 spectrometer. Photoluminescence (PL) spectra were taken using an (Edinburgh Instruments) FLS920 spectrophotometer. Absolute PL quantum yields and fluorescence lifetime were collected on an (Edinburge Instruments, England) FLS 980 spectrometer. Scanning electron microscope (SEM) images were obtained with a Zeiss Merlin (Zeiss Co., Germany) emission scanning electron microscope. Particle size was got by dynamic light scattering (DLS) method on a Brookhaven BI-90 plus particle size analyzer. Single crystal X-ray diffraction (XRD) patterns were taken on a Xcalibur Nova (Agilent Technologies (China) Co., Ltd) diffractometer. The geometrical and electronic structures were obtained at the B3LYP/6-31G** level. Cell viability was analyzed with a Flex Station 3 microplate reader (Moleculardevices, America). Cell imaging performance was examined on a laser scanning confocal microscopy 710 (Zeiss, Germany).

2.2. Synthetic procedures

The molecular structures and synthesis routes of 13-substituted berberine are exhibited in Scheme 1. All the derivatives had a high-quality synthesis and marked as compounds **1-5** (Table 1). Additionally, an oxidation reaction using N-bromosuccinimide (NBS) gave the reaction products **2-5** in good yield [26,27]. 13-hydroxyberberine chloride was synthesized by a sequence of nucleophilic substitution reactions with acetone and $KMnO_4$.

2.2.1. Compound *1*

Berberine chloride (3.71 g, 10 mmol) was dissolved in deionized water (4 mL) and acetone (4 mL). 50 wt% NaOH (5.6 mL) was added in the mixture with vigorous stirring at the room temperature for 30 min. The mixture was filtered and the residue was washed with deionized water (15 mL) and methanol (15 mL) to obtain brown intermediate **6a** (3.85 g, yield: 53%).

The suspension of compound **6a** (2.32 g, 5.9 mmol) was dissolved in acetone (100 mL) and cooled to minus ten degrees

Table 1
Structures of compounds **1-5**.

Compound	R^1	X
1	OH	Cl
2	CH_3	Cl
3	C_2H_5	Cl
4	CH_2Ph	Br
5	CH_2PhCH_3	Br

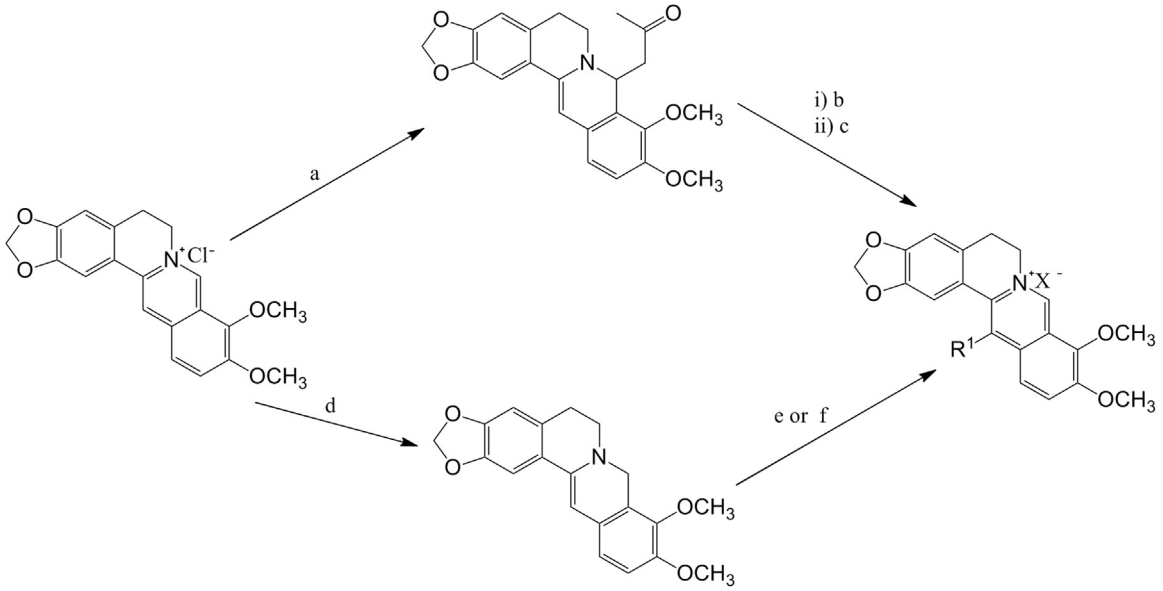

Scheme 1. Synthetic routes of 13-substituted berberine derivatives. (a) acetone, 50 wt% NaOH, room temperature; (b) $KMnO_{4(aq)}$, acetone, −10 °C; (c) HCl $_{(concd)}$, methanol, reflux; (d) $NaBH_4$, K_2CO_3, methanol, room temperature; (e) RCHO, HOAc, 80% ethanol, 85–95 °C; (f) $RPhCH_2Br$, NaI, CH_3CN, room temperature, reflux, NBS.

in the ice-salt bath. $KMnO_4$ (1.1 g, 7 mmol) was added in deionized water (100 mL). $KMnO_4$ solution was dropped dropwise into the reaction system, stirring and maintaining the temperature at minus ten degrees for 2 h. Next, the mixture was filtered and the filter liquor was rotary evaporated to dry. The solid was redissolved in methanol (40 mL), adding concentrated hydrochloric acid (2.5 mL) afterwards. The suspension was heated to reflux for 1.5 h. The solvent was removed by evaporation and recrystallized with ethanol, affording compound **1** (1.2 g, yield: 52%). Yellow powders. ^{1}H and ^{13}C NMR spectra and HRMS-EI analysis are supplied in Fig. S1 for compound **1**. ^{1}H NMR (400 MHz, CH_3OD): δ = 9.42 (s, 1H), 8.23 (d, J = 9.3 Hz, 1H), 8.07 (d, J = 9.4 Hz, 1H), 7.99 (s, 1H), 6.95 (s, 1H), 6.07 (s, 2H), 4.84 (t, J = 8.0 Hz, 2H), 4.18 (s, 3H), 4.11 (s, 3H), 3.17 (t, J = 8.0 Hz, 2H). ^{13}C NMR (100 MHz, CH_3OD): δ = 152.4, 150.6, 150.6, 148.4, 145.8, 138.2, 132.7, 127.6, 127.3, 125.8, 123.7, 120.8, 119.4, 110.4, 109.0, 103.3, 62.5, 58.6, 57.5, 29.0. HMRS (EI–MS); m/z calcd for $C_{20}H_{18}NO_5$ [M-Cl]$^+$: 352.1185; found: 352.1166.

2.2.2. Compound **2**

Berberine chloride (5.57 g, 15 mmol) and K_2CO_3 (5.4 g, 45 mmol) were mixed with methanol (188 mL), then 5 wt% NaOH (7.5 mL) solution containing $NaBH_4$ (0.45 g, 11.3 mmol) was added in small portions and stirred at room temperature. After 1.5 h, precipitation was filtered, washed and recrystallized with ethanol to obtain a dark green intermediate **6b** (3.75 g, yield: 68%).

Compound **6b** (255 mg, 10 mmol) was dissolved in 80% ethanol (12 mL) and acetic acid (3 mL), formaldehyde solution (3 mL) was added. The mixture was heated to 90–95 °C for 4 h. The solvent was evaporated to crude and acidified by 2 M hydrochloric acid (7.5 mL) with stirring at room temperature for 1 h. Precipitation by filtration purified by silica gel chromatography, affording the compound **2** (110 mg, yield: 41%). Yellow powders. ^{1}H and ^{13}C NMR spectra and HRMS-EI analysis are supplied in Fig. S2 for compound **2**. ^{1}H NMR (400 MHz, DMSO-d_6): δ = 9.88 (s, 1H), 8.19 (m, 2H), 7.47 (s, 1H), 7.15 (s, 1H), 6.18 (s, 2H), 4.82 (t, J = 5.6 Hz, 2H), 4.10 (s, 6H), 3.11 (s, J = 5.6 Hz, 2H), 2.93 (s, 3H). ^{13}C NMR (100 MHz, DMSO-d_6): δ = 150.8, 149.4, 146.9, 144.6, 144.4, 136.4, 134.2, 133.5, 130.5, 126.5, 121.8, 121.2, 120.8, 111.1, 108.6, 102.5, 62.5, 57.5, 57.2, 27.8, 18.1. HMRS (EI–MS); m/z calcd for $C_{21}H_{20}NO_4$ [M-Cl]$^+$: 350.1392; found: 350.1370.

2.2.3. Compound **3**

Compound **3** was obtained from intermediate **6b** using the similar procedure as compound **2**. Yield: 42%. Yellow powders. ^{1}H and ^{13}C NMR spectra and HRMS-EI analysis are supplied in Fig. S3 for compound **3**. ^{1}H NMR (400 MHz, DMSO-d_6): δ = 9.93 (s, 1H), 8.24 (d, J = 9.6 Hz, 1H), 8.20 (d, J = 9.6 Hz, 1H), 7.30 (s, 1H), 7.17 (s, 1H), 6.19 (s, 2H), 4.82 (t, J = 5.2 Hz, 2H), 4.10 (s, 3H), 4.10 (s, 3H), 3.37 (q, J = 7.2 Hz, 2H), 3.09 (t, J = 5.6 Hz, 2H), 1.46 (t, J = 7.2 Hz, 3H). ^{13}C NMR (100 MHz, DMSO-d_6): δ = 150.1, 149.0, 146.5, 144.4, 144.3, 135.5, 135.2, 134.0, 132.0, 126.0, 121.2, 121.2, 120.1, 108.8, 108.3, 102.0, 62.0, 57.0, 56.9, 27.3, 22.4, 15.4. HMRS (EI–MS); m/z calcd for $C_{22}H_{22}NO_4$ [M-Cl]$^+$: 364.1549; found: 364.1531.

2.2.4. Compound **4**

A suspension of NaI (465 mg, 3.09 mmol) in acetonitrile (24 mL), benzyl bromide (525 mg, 3.09 mmol) was added dropwise with stirring at room temperature for 1.5 h. Then, the mixture was heated to reflux after adding the intermediate **6b**. Three hours later, reaction system was filtered and the solid was obtained from filtrate by rotary evaporation. The solid was redissolved in dichloromethane (40 mL) which contains NBS (550.5 mg, 3.09 mmol) and then the mixture was stirred at room temperature for 1 h. Evaporating the solvent and purifying the residue by silica gel chromatography, affording the compound **4** (910 mg, yield: 70%). Yellow powders. ^{1}H and ^{13}C NMR spectra and HRMS-EI analysis are supplied in Fig. S4 for compound **4**. ^{1}H NMR(400 MHz, DMSO-d_6): δ = 10.05 (s, 1H), 8.10 (d, J = 9.6 Hz, 1H), 7.79 (d, J = 9.6 Hz, 1H), 7.27–7.39 (m, 3H), 7.17–7.18 (m, 3H), 6.98 (s, 1H), 6.08 (s, 2H), 4.89 (t, J = 4.8 Hz, 2H), 4.76 (s, 2H), 4.13 (s, 3H), 4.03 (s, 3H), 3.16 (t, J = 5.2 Hz, 2H). ^{13}C NMR (100 MHz, DMSO-d_6): δ = 150.7, 149.7, 146.9, 145.9, 144.8, 139.6, 137.7, 134.5, 133.3, 130.5, 129.5, 128.5, 127.2, 126.7, 122.1, 121.7, 120.5, 108.9, 108.6, 102.5, 62.6, 57.5, 36.0, 27.8. HMRS (EI-MS); m/z calcd for $C_{27}H_{24}NO_4$ [M-Cl]$^+$: 426.1705; found: 426.1679.

2.2.5. Compound **5**

Compound **5** was obtained from intermediate **6b** using the similar procedure as compound **4**. Yield: 69%. Yellow powders. ^{1}H and ^{13}C NMR spectra and HRMS-EI analysis are supplied in Fig. S5 for compound **5**. ^{1}H NMR(400 MHz, DMSO-d_6): δ=10.04 (s, 1H), 8.09 (d, J = 9.6 Hz, 1H), 7.76 (d, J = 9.2 Hz, 1H), 7.05–7.18 (m, 6H), 6.99 (s, 1H), 6.08 (s, 2H), 4.89 (t, J = 4.8 Hz, 2H), 4.69 (s, 2H), 4.13 (s, 3H), 4.03 (s, 3H), 3.16 (t, J = 5.6 Hz, 2H), 2.29 (s, 3H). ^{13}C NMR (100 MHz, DMSO-d_6): δ = 150.7, 149.7, 146.9, 145.9, 144.8, 137.6, 136.5, 136.4, 134.5, 133.3, 130.7, 130.1, 128.4, 126.7, 122.1, 121.7, 120.5, 108.9, 108.6, 102.5, 102.5, 62.6, 35.7, 27.76, 2. HMRS (EI-MS); m/z calcd for $C_{28}H_{26}NO_4$ [M-Cl]$^+$: 440.1862; found: 440.1841.

2.3. Nanoaggregates preparation for UV–vis spectra, PL spectra, SEM and DLS measurements

To obtain the nanosuspensions, a series of stock methanol solutions of these derivatives were prepared with a concentration of 10^{-4} M. Aliquots of the stock solutions were transferred to the 10 mL volumetric flasks. Cautiously adding water dropwise under vigorous stirring, and then the appropriate volume of methanol was added. Not only did we keep the constant of final concentration at 10^{-5} M, but also the change of different water fractions from 0 to 90 vol% was unified [28]. Once completed this preparation, UV–vis absorption and PL spectra were measured immediately with the excitation wavelengths of 307, 336, 336, 339, and 339 nm for compounds **1-5** respectively in CH_3OH/H_2O mixture. Through adjusting the pH values from 1 to 12 in CH_3OH/H_2O (10/90 v:v) mixture of compound **1**, the PL intensity spectra with different pH values were obtained. The absolute PL quantum yields (Φ_F) of CH_3OH, CH_3OH/H_2O (2:8 v:v) mixture and CH_3OH/H_2O (1:9 v:v) mixture were recorded on an integrating sphere and fluorescence lifetime of CH_3OH, CH_3OH/H_2O (2:8 v:v) mixture and CH_3OH/H_2O (1:9 v:v) mixture were measured by FLS 980 spectrometer. After standing for 24 h, drops of different proportion of CH_3OH/H_2O (5:5, 2:8, 1:9 v:v) mixture were put onto a silicon wafer by slow evaporation over 12 h at room temperature, metal spraying after completely dry for SEM [29]. Size distribution of compound **1** in CH_3OH/H_2O (5:5, 2:8, 1:9 v:v) mixture after 24 h storage was evaluated with DLS method.

2.4. X-ray crystallography

Faint yellow single crystal suited for X-ray structural analysis was obtained by slow evaporation the mixture of CH_3OH/H_2O (7:1 v:v) in room temperature. All data were measured at low temperature T = 100 (2) K on a Xcalibur Nova (Agilent Technologies (China) Co., Ltd) diffractometer. The structure was got by direct methods (SHELXS 97) and non-hydrogen atoms were refined anisotropically using the least-squares method on F^2. Crystallographic data of 13-hydroxyberberine are in CIF files and deposited into the Cambridge Crystallographic Data Center as supplementary publication number CCDC 1511256, via http://www.ccdc.cam.ac.uk/

2.5. Theoretical calculation

The orbital distribution of highest occupied molecular orbital (HOMO) and lowest unoccupied molecular orbital (LUMO) energy

of compound **1** was calculated using density functional theory (DFT) at the B3LYP/6-31G** level implemented with Gaussian 03.

2.6. Cell viability evaluation

HepG2 cells were seeded in 96-well microplates at a density of 2.5×10^4 cells per mL in 200 μL of the respective media containing 10% fetal bovine serum (FBS), 10 μg/ml of streptomycin and 10 μg/ml penicillin. After 24 h of cell attachment, HepG2 cells were incubated with 10, 20, 40, 80 and 100 μM of compound **1** for 8 and 24 h. Then the cells were washed with phosphate buffered saline (PBS) buffer for three times. Thereafter, 0.5% MTT and 200 μL of Dulbecco's Modified Eagle's Medium (DMEM) cell culture media was added to each well and incubated for 2 h at 37 °C. Plates were then analyzed with a microplate reader (Moleculardevices, America). Measurements of absorbance were carried out at 450 nm.

2.7. Cells culture

Cell imaging of compound **1** in HepG2 cells were obtained on LSM710 laser scanning confocal microscopy (Zeiss, Germany). The excitation wavelength was set as 458 nm. The cells were cultured in DMEM supplemented with 10% fetal bovine serum (FBS). Cell culture was maintained in the medium of 95% air humidity and 5% CO_2 at 37 °C. To maintain the exponential growth of the cells, culture medium had to change every three days. Before treatment, cells were seeded in a glass bottom dish with a density of 1×10^5 cells per dish. The cells were incubated with compound **1** (1000 uL, 100 μM) for 3 h at 37 °C, and the excess was removed by washing three times with phosphate buffered saline (PBS) buffer. Compound **1** was dispersed in the completely cell culture medium.

3. Results and discussion

3.1. Photophysical properties

In Fig. 1a, compounds **2-5** exhibited the approximately absorption spectra profile, which manifest that the length and type of alkyl chain have no significant effect on conjugated backbones. However, the absorption maximum of compound **1** is red-shifted by 32 nm at 445 nm in comparison to others. Reason of the consequence can be attributed to the 13-hydroxy group, which is rich in lone pair electrons increasing the rigidity of molecule by enlarging conjugated system of compound **1** in CH_3OH. Increasing the rigidity of molecule can enhance the fluorescence emission. As shown in Fig. 1b, the excitation wavelengths for compounds **2-5** are nearly 336 nm and 307 nm for compound **1**, the emission trend roughly remains unchanged due to the same luminescent ability of nanoaggregates. In Fig. 1b, the emission maximums are 524 nm, 511 nm, 512 nm, 513 nm and 514 nm for compounds **1-5** respectively, and the PL intensity spectra reveal two distinct emissive bands, approximately at ~373 nm (for compound **1**), ~426 nm (for compounds **2-5**) and ~520 nm (for all compounds). The high-energy band (~520 nm) is ascribed to a TICT emission, while the low-energy bands (~373 nm and 426 nm) are assigned to the emission of the local state [30]. Comparative absorption and emission spectra of compounds **1-5** are represented in Fig. 1.

3.2. Aggregation-induced emission enhancement

In Fig. 2(1a), absorbance of compound **1** slowly decreases with the increasement of water fractions due to Mie effect, which reduces the light transmission in the nanosuspensions. The refined structures of absorption spectrum gradually disappear at 370 nm and a red shift with 9 nm appears at 445 nm that indicates the formation of nanoaggregates of compound **1** [31,32]. There is a slight red shift with 6 nm in Fig. 2(1b) with water fractions changing from 0% to 80%. It is presumable that the number of single light-emitting molecules in nanoaggregates has increased. The fluorescence emission reaches its maximum value at 80% water fraction, which is 1.7-fold higher than pure methanol. The photograph of compound **1** in CH_3OH/H_2O mixtures with different water fractions (0–90 vol%) under UV illumination at 365 nm is shown in Fig. 3. However, the PL intensity of compound **1** decreases when the water fraction reaches 90% with main emission peak at 524 nm in Fig. 2(1b). There are possible guesses for this phenomenon. On the one hand, the molecules change the mode of packing [33]. Nanoaggregates form in an orderly fashion when water fraction ≥80%, like crystal particles. It assembles in a casual way when water fraction ≥90%, like amorphous particles. On the other hand, nanoaggregates tend to form greater particles even precipitation, which decrease the concentration of light-emitting nanoaggregates and weakens its fluorescence emission [34]. The absorption spectra (Fig. 2(2a–5a)) of compounds **2-5** in CH_3OH/H_2O mixture show that there are no significantly changes on absorbance with the change of water fractions. Therefore, it is difficult to clearly distinguish these curves and can't use arrows to

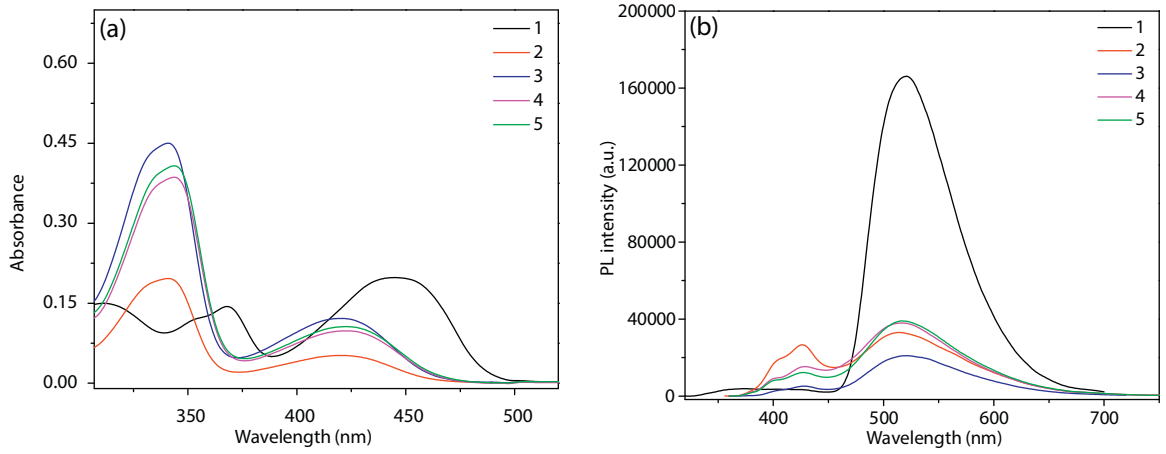

Fig. 1. Absorption (a) and PL (b) spectra with the excitation wavelength of 307, 336, 336, 339, and 339 nm for compounds **1-5** with a concentration of 2.07×10^{-5} M in methanol, respectively.

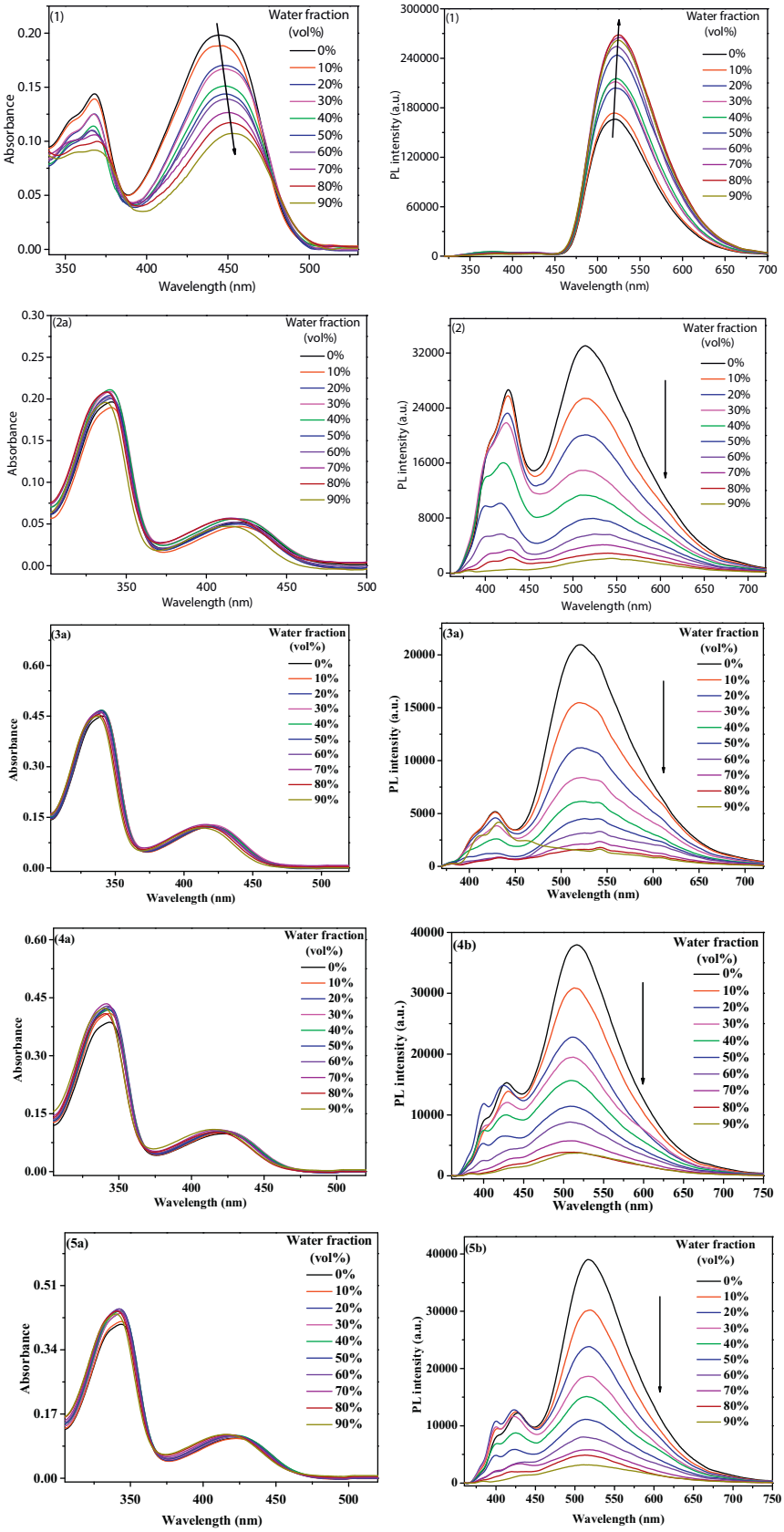

Fig. 2. Absorption (1a–5a) and PL spectra (1b–5b) of compounds **1-5** ($c = 2.07 \times 10^{-5}$ M) in CH_3OH/H_2O mixtures with different water fractions (0–90 vol%). Arrows illustrate the peak changes.

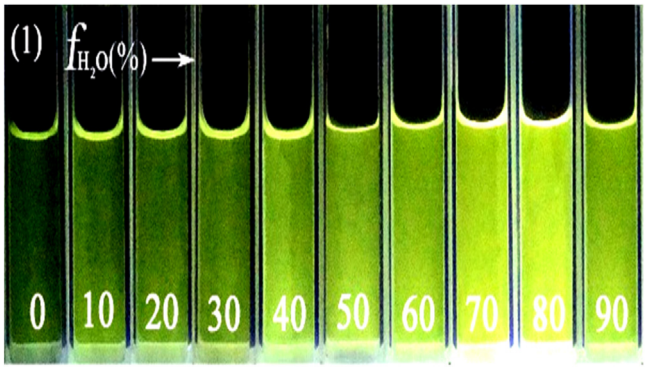

Fig. 3. Photograph of compound **1** in CH_3OH/H_2O mixtures with different water fractions (0–90 vol%) under UV illumination at 365 nm.

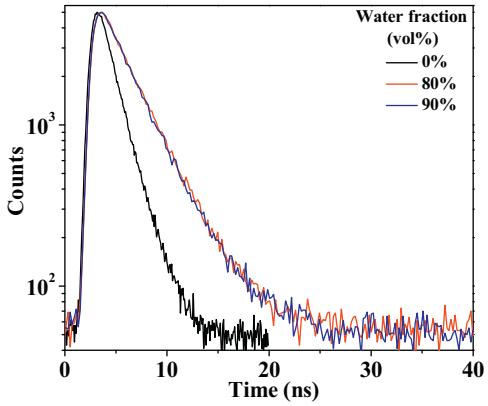

Fig. 4. Time-resolved fluorescence curves in CH_3OH, CH_3OH/H_2O (2:8 v:v) mixture and CH_3OH/H_2O (1:9 v:v) mixture. The fluorescence lifetime is 1.67 ns, 3.16 ns and 3.10 ns, respectively.

illustrate the changes of absorbance. In Fig. 2(2b–5b), PL intensity decreases with the increasement of water fractions, which is characterized for ACQ behavior, and the photographs of compound **2-5** in CH_3OH/H_2O mixtures with different water fractions (0–90 vol%) under UV illumination at 365 nm are supplied in Fig. S6.

Results reveal that 13-hydroxyberberine chloride is an AIEE active compound, while compounds **2-5** suffer from aggregation-caused quenching (ACQ). To have a quantitative comparison, the fluorescence quantum yields (Φ_F) of compounds **1-5** in the CH_3OH were measured by using an integrating sphere, which are 3%, 2%, 4% and 6% respectively in Table 2. Besides, the fluorescence quantum yields (Φ_F) of compound **1** in CH_3OH/H_2O (2:8 v:v) mixture and CH_3OH/H_2O (1:9 v:v) mixture are 8, 27, and 17% respectively, which is accord with the behavior of PL intensity spectrum. Time resolved fluorescence spectra of compound **1** were measured in CH_3OH, CH_3OH/H_2O (2:8 v:v) mixture and CH_3OH/H_2O (1:9 v:v) mixture by a time-resolved technique. As shown in Fig. 4, the emission enhancement of compound **1** in CH_3OH and CH_3OH/H_2O mixtures is in accordance with a corresponding change in lifetime. The fluorescence lifetime in CH_3OH/H_2O (2:8 v:v) mixture is 3.16 ns, which is longer than that in the CH_3OH (1.67 ns) and CH_3OH/H_2O (1:9 v:v) mixture (3.10 ns). The results are similar to the emission fluorescence behavior of compound **1** in different water fractions. The transition time in CH_3OH is very fast, leading to low fluorescence quantum yield and emission fluorescence intensity.

Nanoaggregates of compound **1** with different water fractions were observed by scanning electron microscope (SEM) and their particle sizes distribution were measured by dynamic light scattering (DLS) method. In Fig. 5a–c, many small uniform globular nanoaggregates with different sizes form in all mixtures of CH_3OH/H_2O (5:5 v:v), CH_3OH/H_2O (2:8 v:v) and CH_3OH/H_2O (1:9 v:v). As shown in Fig. 5d, particle size of nanoaggregates mainly distributes at 140 nm in CH_3OH/H_2O (5:5 v:v) mixture. Molecules aggregate into smaller globular nanoparticles with particle size round 100 nm in CH_3OH/H_2O (2:8 v:v) mixture (Fig. 5e) compared with CH_3OH/H_2O (5:5 v:v) mixed solution. The reason why the diameter of nanoaggregates decrease with the increasement of water fraction is that more compact aggregation formed in high water fraction. In Fig. 5f, most of nanoparticles distribute at 170 nm even adhesion to each other in the mixture of CH_3OH/H_2O (1:9 v:v). Therefore, we can conclude that the formation of smaller dimensions nanoaggregates results in strong emission with increasing the water fractions until 80%, which is identical to the behavior of PL intensity spectrum [35–37].

In order to further explore the AIEE property of compound **1** in different morphology, a series of PL spectra were investigated in the pure solution, mixed solution with f_w = 80%, amorphous and single crystal state. In Fig. 6, emission wavelengths at 540 nm and 554 nm are observed for the amorphous and the crystal respectively, which are obvious red shift with 16 nm and 30 nm compared with the λ_{em} = 524 nm in the pure solution and mixed solution. In comparison to the solution, the red shift emission of the amorphous and the crystal are possibly caused by the strong J-aggregation. For a clearly comparison, the fluorescence quantum yields (Φ_F) of compound **1** in the pure solution, mixed solution with f_w = 80%, amorphous and single crystal state were measured by using an integrating sphere, which are 8%, 27%, 30% and 41% respectively (Table 3). Furthermore, single crystal was prepared and analyzed to elucidate this phenomenon.

Table 2
Photophysical data of compound **1**.

Compound	Solvent	Absorption[a] $\lambda_{max(abs)}$ (nm)	Emission[a] $\lambda_{max(em)}$ (nm)	Stokes shift[b] (cm^{-1})	Quantum yield Φ_F [a]
1	CH_3OH	445	520	3241	0.08
	CH_3OH/H_2O (2:8 v:v)	451	524	3089	0.27
	CH_3OH/H_2O (1:9 v:v)	454	522	2869	0.17
2	CH_3OH	420	511	4240	0.03
3	CH_3OH	421	513	4221	0.02
4	CH_3OH	424	513	4092	0.04
5	CH_3OH	425	514	4071	0.06

[a] Recorded in CH_3OH, CH_3OH/H_2O (2:8 v:v), CH_3OH/H_2O (1:9 v:v) ($c = 2.07 \times 10^{-5}$ M) at 25 °C.
[b] Stokes shift = $\lambda_{max(abs)} - \lambda_{max(em)}$ (cm^{-1}).

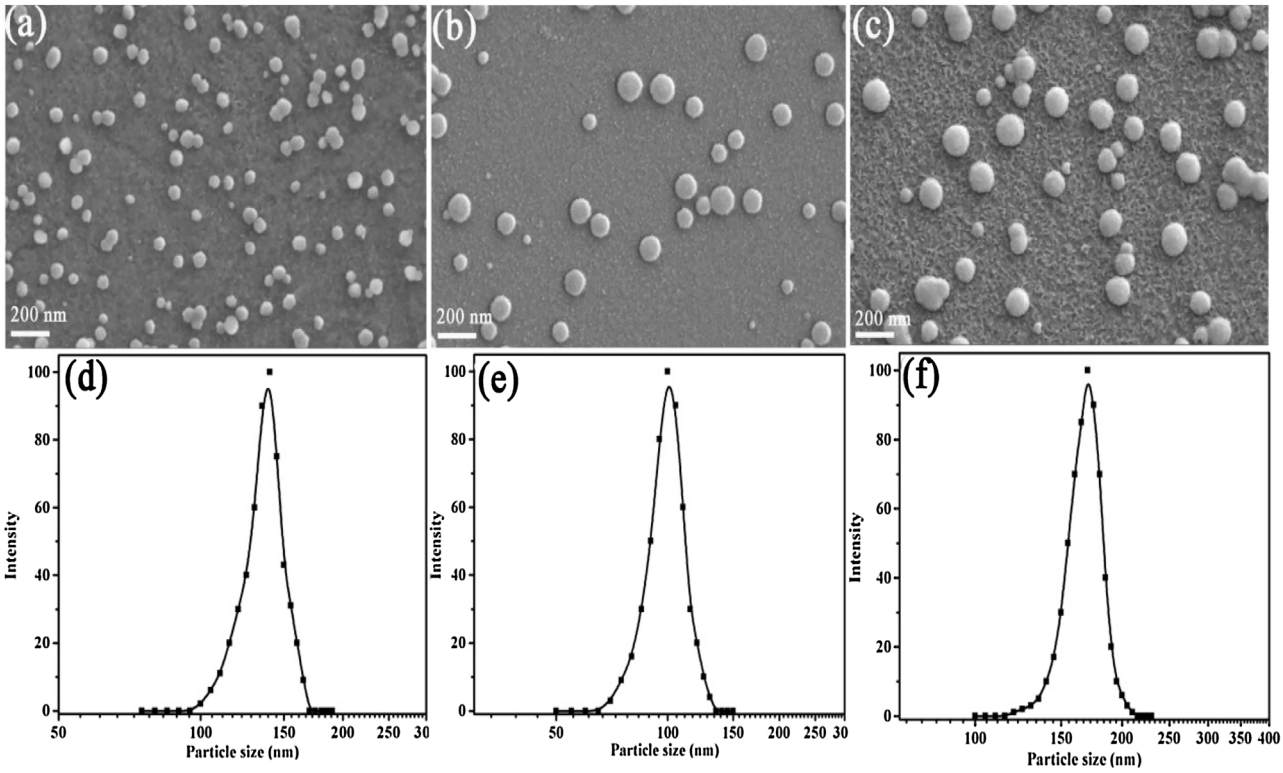

Fig. 5. (a) SEM image of compound **1** in CH_3OH/H_2O (5:5 v:v) mixture; (b) SEM image of compound **1** in CH_3OH/H_2O (2:8 v:v) mixture; (c) SEM image of compound **1** in CH_3OH/H_2O (1:9 v:v) mixture; (d) DLS image of compound **1** in CH_3OH/H_2O (5:5 v:v) mixture; (e) DLS image of compound **1** in CH_3OH/H_2O (5:5 v:v) mixture; (f) DLS image of compound **1** in CH_3OH/H_2O (5:5 v:v) mixture.

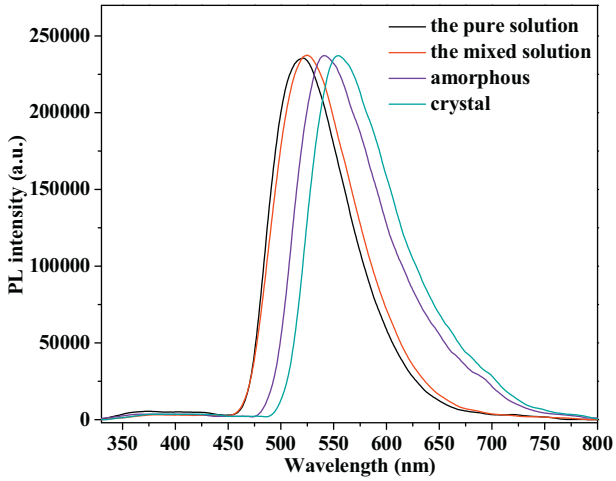

Fig. 6. PL spectra of compound **1** in the pure solvent, the mixed solvent with f_w = 80%, the amorphous and the crystal.

Table 3
Photophysical data of compound **1** with different morphology.

Morphology	Emission $\lambda_{max(em)}$ (nm)	Quantum yield Φ_F
Solution	522	0.08
Aggregation	524	0.27
Amorphous	540	0.30
Crystal	554	0.41

3.3. Crystal structure

To have a further understanding of the mechanism, all the compound were prepared for single crystal growth by vaporizing mixed solvents of methanol and pure water (7:1 v:v) at room temperature. However, only compound **1** produced crystal. The molecular stacking mode of the crystal was explored by X-ray diffraction on a Xcalibur Nova (Agilent Technologies (China) Co., Ltd). Empirical absorption corrections were applied automatically. The structures were solved with direct methods and refined with a full-matrix least-squares technique. Crystallographic data are summarized in Table 4 and the supplementary publication number CCDC is 1511256. The unit cell of compound **1** is triclinic, space group *P*-1, containing two discrete molecules. The ORTEP diagrams with the N and O atom numbering schemes and packing interactions in the crystal of compound **1** are depicted in

Table 4
Crystallographic data and refinement parameters for compound **1**.

Compound **1**			
chemical formula	$C_{21}H_{21}NO_6$	volume (Å^3)	880.93(8)
formula wt	383.39	*Z*	2
temperature (K)	100(2)	density (g/cm^3)	1.445
crystal size (mm^3)	0.50 × 0.1 × 0.08	2θ range	4.7790–71.6280
crystal system	triclinic	F (000)	404
space group	*P*-1	no. of reflns	6321
a (Å)	9.0561(5)	no. of unique reflns	2911
b (Å)	9.2618(5)	no. of params	257
c (Å)	11.3096(7)	R_{all}, R_{obs}[a]	0.0415, 0.0370
α (deg)	87.223(4)	$wR_{2,all}$, $wR_{2,obs}$[b]	0.1002, 0.0957
β (deg)	68.861(5)	Goodness-of-fit on F^2	1.050
γ (deg)	84.744(4)		

$w = 1/[\sigma^2(F_o)^2 + (aP)^2 + bP]$, where $P = [(F_o^2) + 2F_c^2]/3$.
[a] $R_1 = \Sigma||F_o| - |F_c||/\Sigma|F_o|$.
[b] $wR_2 = [\Sigma[w(F_o^2 - F_c^2)^2]/\Sigma w(F_o^2)^2]^{1/2}$.

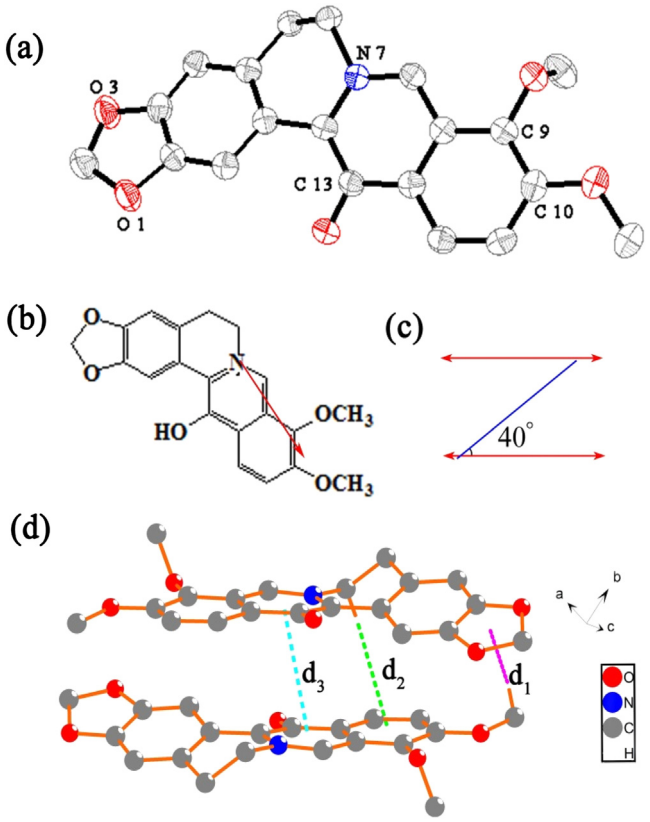

Fig. 7. (a) ORTEP diagram of compound **1**, (b) Dipolar orientation of compound **1**, (c) Slip angle of compound **1**, (d) Packing arrangement and C—H···π interaction in the adjacent molecules marked by dashed line (purple), (hydrogen atoms except H8 and CH_3OH solvent are omitted for charity).

Fig. 7a. As shown in Fig. 7b, the arrow on the molecule shows the dipolar orientation. Due to the planar heterocycles, the molecule tends to form the parallel conformation with the neighboring one, which gives rise to molecular planarization to some extent. It is also the reason why absorption band doesn't become narrowed of compound **1**. The molecular dimer is stacked in "head-to-tail" mode that is J-aggregation with slip angle θ of 40° (Fig. 7c), which creates an advantage on the enhancement of fluorescence emission in aggregation state. In Fig. 7c, the distance between adjacent molecules is d_3 = 3.80 Å, which is too large to form strong π-π interaction. A kind of C—H···π hydrogen bond forms between two molecules with the angle and interaction distance (d_1) are 3.33 Å and 132°, where the dimethoxy groups of one molecule acts as H donor and the [1,3]dioxolane acts as H acceptor. Other C—H···π hydrogen bond isn't formed because of the large distance d_2 = 3.62 Å. There is a weak interdipole interaction for compound **1**, which will decrease the aggregation-caused quenching. In a word, the AIEE mechanism of compound **1** is the result of J-aggregation combined with molecular planarization [38–40].

3.4. Electronic structure

To understand the relationship between the optical property and electronic structure, the highest occupied molecular orbital (HOMO) and lowest unoccupied molecular orbital (LUMO) of compound **1** was optimized using density functional theory (DFT) at the B3LYP/6-31G** level. The HOMO energy level for compound **1** was calculated as −8.75 eV. Meanwhile, the LUMO energy level was calculated to be −5.65 eV, and the calculated band gap is 3.10 eV, As shown in Fig. 8, HOMO and LUMO of compound **1** are mainly localized on dimethoxy unit and isoquinoline part,

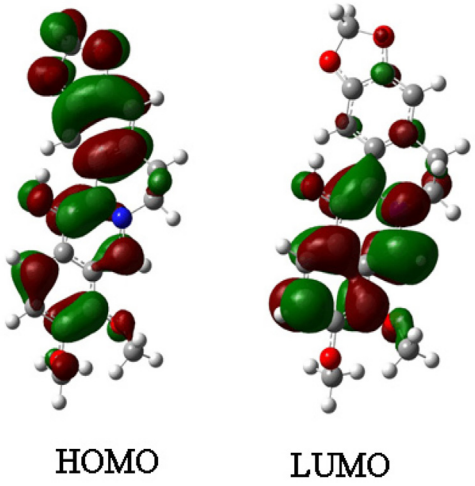

Fig. 8. Energy level and electron density distribution of frontier molecular orbital of compound **1**.

respectively, which leads to two adjacent molecules stacking in "head-to-tail" mode that is J-aggregation consisting with the crystal structure. The theoretical study also explains the AIEE property of compound **1**.

3.5. pH fluorescence probe

On the basis of above exploration, 13-hydroxyberberine chloride has been proved possessing the effect of aggregation-induced emission enhancement, which has an advantage over traditional probes with the problem of aggregation-caused quenching (ACQ). So its pH sensitivity was studied to find if it has the potential value as pH fluorescence probe. A series of mixed solution CH_3OH/H_2O (1:9 v:v) of compound **1** with different pH values was prepared and pH values were adjusted by a spot of dilute hydrochloric acid and dilute sodium hydroxide from 1 to 12. As shown in Fig. 9a, the PL intensity increases slowly when pH values < 5.52, while it increases remarkably when pH values > 5.52. PL intensity maximum appears at pH = 6.84 because the molecules of compound **1** forms a number of nanoparticles, which is 5-fold higher than pH = 1.57. Nonetheless, PL intensity gradually decreases when pH > 6.84. It is reasonable to infer that 13-hydroxy group of compound **1** is transformed into sodium alkoxide salt, which results in a portion of compound **1** dissolves in the solvent, reducing the formation of nanoaggregates [41–43]. Experimental results show that compound **1** has sensitive response to the changes of pH values, especially under the low-acid environment. pK_a value is a main parameter of pH fluorescence probe, which determines the appropriate pH detection range. Additionally, a bit of pH variation can cause the obvious changes of PL intensity around the pKa value. In Fig. 8b, pK_a value can be confirmed as 5.12 when I/I_{max} = 0.5 (in Fig. 9b).

Cell viability is an important parameter, which decides the biological application potential for biological probe. As shown in Fig. 10, the cytotoxicity of compound **1** in HepG2 cells was examined by MTT assay [44,45]. It can be found that the cell viability values have not changed apparently after cells were incubated with different concentrations (10, 20, 40, 80 and 100 μM) of compound **1** for 8 and 24 h. These values are greater than 95% and some even greater than 100%. Result suggests that compound **1** has a high potential for biological probe. Considered the strong fluorescence and high cell viability, the cell uptake behavior of compound **1** was evaluated using laser scanning confocal microscopy (LSM) to explore their potential biological

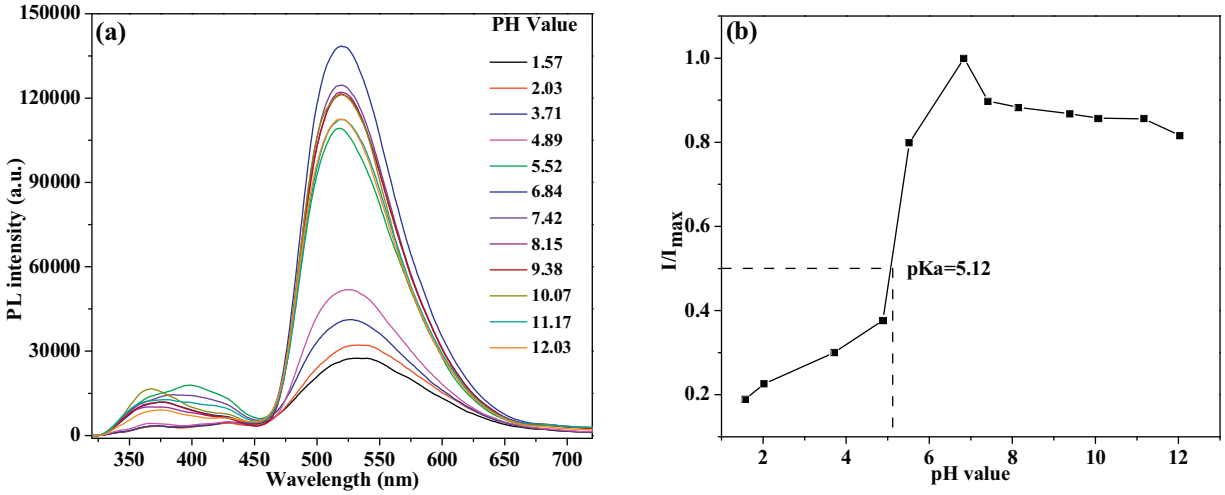

Fig. 9. (a) The changes of PL intensity with different pH values of compound **1** ($c = 2.07 \times 10^{-5}$ M) in CH_3OH/H_2O (1:9 v:v) mixtures. (b) The changes of relative PL intensity versus pH values. The excitation wavelength is 307 nm.

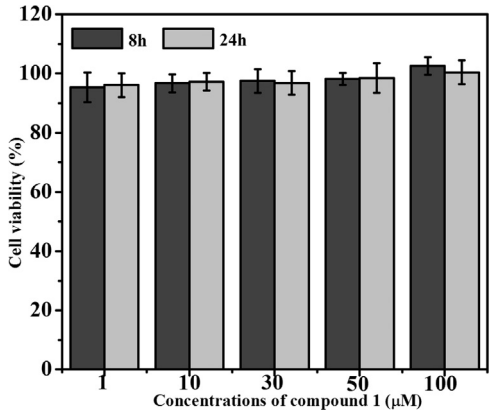

Fig. 10. Cell viability of compound **1**. HepG2 cells were incubated with 1–100 μM of compound **1** for 8 and 24 h.

imaging application. As shown in Fig. 11, an intracellular fluorescent was observed in the location of HepG2 cells after compound **1** was incubated with the concentration of 100 μM for 3 h. The distribution of the probe within the cells was observed by high resolution confocal fluorescent microscope. Compound **1** could be internalized by HepG2 cells and distributed in the whole cells. Hence, it can be inferred that the compound **1** maybe locate at a substance, which widely distributes in the cells. Therefore, the specific action target between compound **1** and HepG2 cells will be explored in our later works. In addition, normal morphology of cells was kept and adhered very well to the cell plates in Fig. 11b, which suggests that compound **1** possesses biocompatibility.

4. Conclusion

In conclusion, a series of berberine derivatives at 13-position (compounds **1-5**) has been designed and synthesized. AIEE phenomenon happened when the substituent is hydroxy group at 13-position, while others show weak fluorescence in nano-aggregation state. Optical spectra of five kinds of derivatives were obtained in aqueous suspension and 13-hydroxyberberine chloride shows AIEE phenomenon owing to nanoaggregates formation. A great deal of small globular nanoaggregates of compound **1** was observed in SEM images and its particle sizes were obtained by DLS method, which is in favor of fluorescence emission. Crystal structure of compound **1** was achieved through the X-ray diffraction analysis. Crystallographic data shows that J-aggregation combined with molecular planarization are observed in the crystal, which is the mechanism of fluorescence emission enhancement. DFT calculation on HOMO and LUMO is consistent with the AIEE property of compound **1**. All results suggest that the aggregation-induced emission enhancement property is influenced by substituent. Moreover, compound **1** has excellent pH sensitivity, and the LSM images showed that compound **1** can be easily internalized by HepG2 cells, which implies its potential as pH fluorescence probe.

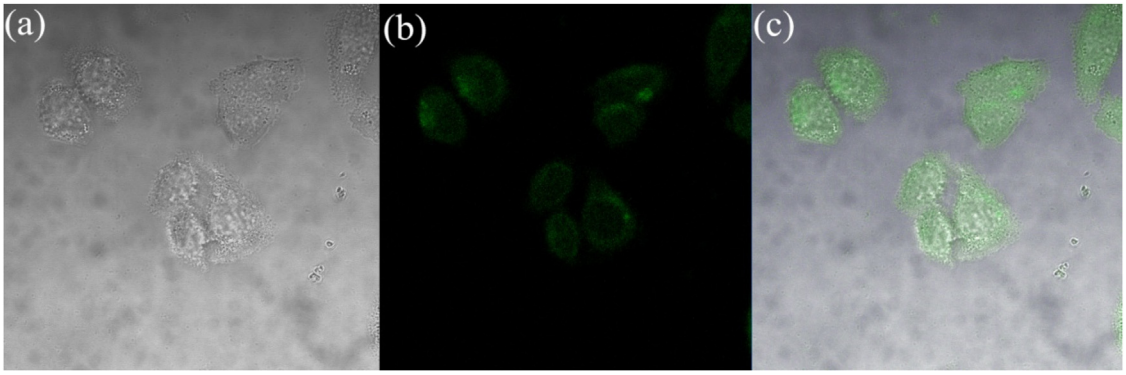

Fig. 11. LSM images of HepG2 cells. Cells were incubated with 100 μM of compound **1** for 3 h. (a) Bright field, (b) Fluorescent image, (c) The overlap image of a and b. The HepG2 cells were excitated with a laser with at 458 nm.

The structure of 13-hydroxyberberine will be modified to decrease its effective concentration when applied to biological application and its specific action target between compound **1** and HepG2 cells will be explored in our following work.

Acknowledgement

This work was supported by the National Natural Science Foundation of China (Grant number: 81173577) and the Natural Science Foundation of Guangdong (8451008901000380).

Appendix A. Supplementary data

Supplementary data associated with this article can be found, in the online version, at http://dx.doi.org/10.1016/j.jphotochem.2017.01.017.

References

[1] B. Bozzini, B. Busson, C. Humbert, C. Mele, A. Tadjeddine, Electrochemical fabrication of nanoporous gold decorated with manganese oxide nanowires from eutectic urea/choline chloride ionic liquid. Part III–electrodeposition of Au-Mn: a study based on in situ sum-frequency generation and Raman spectroscopies, Electrochim. Acta 218 (2016) 208–215.
[2] Z. Chen, J. Zhang, M. Song, J. Yin, G.A. Yu, S.H. Liu, A novel fluorene-based aggregation-induced emission (AIE)-active gold(I) complex with crystallization-induced emission enhancement (CIEE) and reversible mechanochromism characteristics, Chem. Commun. 51 (2015) 326–329.
[3] K. Afshinnia, M. Sikder, B. Cai, M. Baalousha, Effect of nanomaterial and media physicochemical properties on Ag NM aggregation kinetics, J. Colloid Interface Sci. 487 (2017) 192–200.
[4] Y. Huang, Y. Laditskv, On the kinetics of chitosan/tripolyphosphate micro- and nanogel aggregation and their effects on particle polydispersity, J. Colloid Interface Sci. 486 (2017) 27–37.
[5] Z.J. Zhao, J.W.Y. Lam, B.Z. Tang, Tetraphenylethene: a versatile AIE building block for the construction of efficient luminescent materials for organic light-emitting diodes, J. Mater. Chem. 22 (2012) 23726–23740.
[6] J.Z. Liu, J.W.Y. Lam, B.Z. Tang, Aggregation-induced emission of silole molecules and polymers fundamental and application, J. Inorg. Organomet. Polym. Mater. 19 (2009) 249–285.
[7] M.W. Chung, T.Y. Lin, C.C. Hsieh, K.C. Tang, H. Fu, P.T. Chou, S.H. Yang, Y. Chi, Excited-state intramolecular proton transfer (ESIPT) fine-tuned by quinoline-pyrazole isomerism: π-conjugation effect on ESIPT, J. Phys. Chem. A 114 (2010) 7886–7891.
[8] W.A. Morris, K. Milena, C.L. Fraser, Effects of α-substitution on mechanochromic luminescence and aggregation-induced emission of difluoroboron β-diketonate dyes, J. Phys. Chem. C 120 (2016) 22539–22548.
[9] X. Feng, B. Tong, J. Shen, Aggregation-induced emission enhancement of aryl-substituted pyrrole derivatives, J. Phys. Chem. B 114 (2010) 16731–16736.
[10] Z. Zhao, Z. Wang, P. Lu, C.Y.K. Chan, D. Liu, J.W.Y. Lam, H.H.Y. Sung, I.D. Williams, Y. Ma, B.Z. Tang, Structural modulation of solid-state emission of 2, 5-Bis (trialkylsilylethynyl)-3, 4-diphenylsiloles, Angew. Chem. Int. Ed. 48 (2009) 7608–7611.
[11] P. Galer, R.C. Korošec, M. Vidmar, B. Sket, Crystal structures and emission properties of the BF_2 complex 1-phenyl-3-(3,5-dimethoxyphenyl)-propane-1,3-dione: multiple chromisms, aggregation- or crystallization-induced emission, and the self-assembly effect, J. Am. Chem. Soc. 136 (2014) 7383–7394.
[12] S. Varghese, S. Das, Role of molecular packing in determining solid-state optical properties of π-conjugated materials, J. Phys. Chem. Lett. 2 (2011) 863–873.
[13] Y. Niu, Y. Qian, Synthesis and aggregation-induced emission enhancement of naphthalimide-rhodamine dye, J. Photochem. Photobiol. A Chem. 329 (2016) 88–95.
[14] Z. Long, M. Liu, R. Jiang, Q. Wan, L. Mao, Y. Wan, F. Deng, X. Zhang, Y. Wei, Preparation of water soluble and biocompatible AIE-active fluorescent organic nanoparticles via multicomponent reaction and their biological imaging capability, Chem. Eng. J. 308 (2017) 527–534.
[15] M. Held, Y. Zakharko, M. Wang, F. Jakubka, F. Gannott, W. Rumer Joseph, S. Ashraf Raja, I. McCulloch, J. Zaumseil, Org. Electron. 32 (2016) 220–227.
[16] M. Tatsuro, W. Toshiaki, T. Yoko, O. Shuji, Effective polar orientation of organic polar nanocrystals and their fixation in polymer matrices, Jpn. J. Appl. Phys. 53 (2014) (061601/1-061601/7).
[17] Y. Li, J. Han, L. Jiang, F. Li, K. Li, Y. Dong, A glucose biosensor based on immobilization of glucose oxidase on platinum nanoparticle doped santa barbara amorphous material-15, Anal. Lett. 48 (2015) 1139–1149.
[18] L. Feng, W. Shi, J. Ma, Y. Chen, F. Kui, Y. Hui, Z. Xie, A novel thiosemicarbazone Schiff base derivative with aggregation-induced emission enhancement characteristics and its application in Hg^{2+} detection, Sens. Actuators B Chem. 237 (2016) 563–569.
[19] Y. Lin, W. Lin, K. Zheng, S. Zhu, FRET-based small-molecule fluorescent probes: rational design and bioimaging applications, Acc. Chem. Res. 43 (2013) 1462–1473.
[20] A. Shi, L. Huang, C. Lu, F. He, X. Li, Synthesis, biological evaluation and molecular modeling of novel triazole containing berberine derivatives as acetylcholinesterase and b-amyloid aggregation inhibitors, Bioorg. Med. Chem. 19 (2011) 2298–2305.
[21] L. Huang, T. Su, W. Shan, Z. Luo, Y. Sun, F. He, X. Li, Inhibition of cholinesterase activity and amyloid aggregation by berberine-phenyl-benzoheterocyclic and tacrine-phenylbenzoheterocyclic hybrids, Bioorg. Med. Chem. 20 (2012) 3038–3048.
[22] L. Huang, A. Shi, F. He, X. Li, Synthesis, biological evaluation, and molecular modeling of berberine derivatives as potent acetylcholinesterase inhibitors, Bioorg. Med. Chem. 18 (2010) 1244–1251.
[23] J. Chahine, N. Saffon, M. Cantuel, S. Fery-Forgues, Spontaneous formation of fluorescence nanofibers and reticulated solid from berberine palmitate: a new example of aggregation-induced emission enhancement in organic ion pairs, Langmuir 27 (2011) 2844–2853.
[24] L. Zhang, J. Li, F. Ma, S. Yao, N. Li, J. Wang, Y. Wang, Q. Yao, Synthesis and cytotoxicity evaluation of 13-n-alkyl berberine and palmatine analogue as anticancer agents, Molecules 17 (2012) 11294–11302.
[25] D. Bhowmik, M. Hossain, F. Buzzetti, R. D'Auria, P. Lombardi, G.S. Kumar, Biophysical studies on the effect of the 13 position substitution of the anticancer alkaloid berberine on its DNA binding, J. Phys. Chem. B 116 (2012) 2314–2324.
[26] K.D. Park, S.J. Cho, J.S. Moon, S.U. Kim, Synthesis and antifungal activity of a novel series of 13-(4-isopropylbenzyl) berberine derivatives, Bioorg. Med. Chem. Lett. 20 (2010) 6551–6554.
[27] F. Wang, Y. Xu, S.O. Aderinto, H. Peng, H. Zhang, H. Wu, A new highly effective fluorescent probe for Al^{3+} ions and its application in practical samples, J. Photochem. Photobiol. A Chem. 332 (2017) 273–282.
[28] D. Bhowmik, F. Buzzetti, G. Fiorillo, F. Orzi, T.M. Syeda, P. Lombardi, G.S. Kumar, Synthesis of new 13-diphenylalkyl analogues of berberine and elucidation of their base pair specificity and energetics of DNA binding, Med. Chem. Commun. 5 (2014) 226–231.
[29] Y.X. Wang, W.J. Kong, Y.H. Li, S. Tang, Z. Li, Y.B. Li, Y.Q. Shan, C.W. Bi, J.D. Jiang, D. Q. Song, Synthesis and structure-activity relationship of berberine analogues in LDLR up-regulation and AMPK activation, Bioorg. Med. Chem. 20 (2012) 6552–6558.
[30] Y. Ren, W.H. Kan, M.A. Henderson, P.G. Bomben, C.P. Berlinguette, V. Thangadurai, T. Baumgartner, External-Stimuli responsive photophysics and liquid crystal properties of self-assembled phosphole-lipids, J. Am. Chem. Soc. 133 (2011) 17014–17026.
[31] S. Kumar, P. Singh, A. Mahajan, S. Kumar, Aggregation induced emission enhancement in ionic self-assembled aggregates of benzimidazolium based cyclophane and sodium dodecylbenzenesulfonate, Org. Lett. 15 (2013) 3400–3403.
[32] M.D. Lechner, C. Helmut, M. Vikas, V. Antje, W. Wendel, Sedimentation measurements with the analytical ultracentrifuge with absorption optics: influence of Mie scattering and absorption of the particles, Colloid Polym. Sci. 289 (2011) 1145–1155.
[33] M. Campetella, L. Gontrani, E. Bodo, F. Ceccacci, F.C. Marincola, R. Caminiti, Conformational isomerisms and nano-aggregation in substituted alkylammonium nitrates ionic liquids: an x-ray and computational study of 2-methoxyethylammonium nitrate, J. Chem. Phys. 138 (2013) 184506.
[34] Z. Zheng, Z. Yu, M. Yang, F. Jin, Q. Zhang, H. Zhou, J. Wu, Y. Tian, Substituent group variations directing the molecular packing electronic structure, and aggregation-induced emission property of isophorone derivatives, J. Org. Chem. 78 (2013) 3222–3234.
[35] X.Q. Zhang, Z.G. Chi, B.J. Xu, C.J. Chen, X. Zhou, Y. Zhang, S.W. Liu, J.R. Xu, End-group effects of piezofluorochromic aggregation-induced enhanced emission compounds containing distyrylanthracene, J. Mater. Chem. 22 (2012) 18505–18513.
[36] X. Zhu, G. Wu, D. Chen, Molecular dynamics simulation of cyclodextrin aggregation and extraction of Anthracene from non-aqueous liquid phase, J. Hazard. Mater. 320 (2016) 169–175.
[37] S.A. Dergunov, M.D. Kim, S.N. Shmakov, A.G. Richter, W. Steven, P. Eugene, Tuning optical properties of encapsulated clusters of gold nanoparticles through stimuli-triggered controlled aggregation, Chem. A Eur. J. 22 (2016) 7702–7705.
[38] H. Khakpour, M. Abdollahi, A. Nasiri, Synthesis, microstructural characterization and hydrophobic intermolecular nano-aggregation behavior of acrylamide/2-acrylamido-2-methy-1-propane sulfonic acid/butyl acrylate co-and terpolymers, J. Polym. Res. 22 (2015) 189–202.
[39] T.N. Govindaiah, Studies on optical characterization and nano-aggregation of molecules in ternary mixture of liquid crystalline materials, Mol. Cryst. Liq. Cryst. 1 (2015) 74–79.
[40] S.Z.M. Zafaranchi, K. Khoshaman, R. Masoudi, B. Hemmateenejad, R. Yousefi, The structural alteration and aggregation propensity of glycated lens crystallins in the presence of calcium: importance of lens calcium homeostasis in development of diabetic cataracts, Spectrochim. Acta Part A Mol. Biomol. Spectrosc. 170 (2017) 174–183.
[41] Y. Hu, F. Zhao, S. Hua, Y. Dong, D. Li, Z. Su, A novel turn-on colorimetric and fluorescent sensor for Fe^{3+} and its application in living cells, J. Photochem. Photobiol. A Chem. 332 (2017) 351–356.

[42] Y.J. Wang, L. Lin, X. Zhang, V. Schultz, F. Zhang, J.Z. Sun, R.J. Linhardt, Selective, switchable fluorescent probe for heparin based on aggregation-induced emission, Anal. Biochem. 514 (2016) 48–54.
[43] V.G. Avakyan, V.B. Nazarov, A.V. Odinokov, A.V. Koshikin, M.V. Alfimov, Structure and aggregation of β-cyclodextrin-pyrene-analyte supramolecular sensor: absorption/emission spectra and simulations, J. Lumin. 180 (2016) 328–340.
[44] Q. Meng, L.F. Yau, J.G. Lu, Z.Z. Wu, B.X. Zhang, J.R. Wang, Z.H. Jiang, Chemical profiling and cytotoxicity assay of bufadienolides in toad venom and toad skin, J. Ethnopharmacol. 187 (2016) 74–82.
[45] J. Liang, C.L. Fang, W.L. Wu, P.H. Yu, J.Y. Gao, J.B. Li, Preparation and properties evaluation of a novel pH-sensitive liposomes based on imidazole-modified cholesterol derivatives, Int. J. Pharm. 518 (2016) 213–219.